Journal of Applied Physics

Investigation on the optimized design of alternate-hole-defect for 2D phononic crystal based silicon microresonators

Nan Wang, Fu-Li Hsiao, J. M. Tsai, Moorthi Palaniapan, Dim-Lee Kwong et al.

Citation: J. Appl. Phys. **112**, 024910 (2012); doi: 10.1063/1.4740085
View online: http://dx.doi.org/10.1063/1.4740085
View Table of Contents: http://jap.aip.org/resource/1/JAPIAU/v112/i2
Published by the American Institute of Physics.

Investigation on the optimized design of alternate-hole-defect for 2D phononic crystal based silicon microresonators

Nan Wang,[1,2] Fu-Li Hsiao,[1,3] J. M. Tsai,[2] Moorthi Palaniapan,[1] Dim-Lee Kwong,[2] and Chengkuo Lee[1,a)]
[1]*Department of Electrical and Computer Engineering, National University of Singapore, 4 Engineering Drive 3, Singapore 117576*
[2]*Institute of Microelectronics, A*STAR (Agency for Science, Technology and Research), 11 Science Park Road, Singapore 117685*
[3]*Graduate Institute of Photonics, National Changhua University of Education, No. 1, Jin-De Road, Changhua City 500, Taiwan*

(Received 6 April 2012; accepted 27 June 2012; published online 31 July 2012)

This paper shows the design, fabrication, and characterization of the Bloch-mode micromechanical resonators made by creating alternate defects to form a resonant cavity on a two-dimensional silicon phononic crystal slab of square lattice. The length of the resonant cavity (L) and the central-hole radius (r') are varied to optimize the performance of the resonators. CMOS-compatible aluminium nitride is used as the piezoelectric material of the interdigital transducer to launch and detect acoustic waves. The extent of energy confinement within the cavity, as shown by the simulated displacement profiles of the resonators, agrees with the measured Q factors. We also quantitatively analysed the band structure of the proposed resonators and found that the Q factors are generally in an inverse relationship with the standard deviation of the band, due to the slow sound effect brought by flat bands which reduces the energy loss along the lateral direction (Y direction) and enhances the Q factor. *© 2012 American Institute of Physics*. [http://dx.doi.org/10.1063/1.4740085]

I. INTRODUCTION

Phononic crystals (PnCs), also called phononic band gap (PnBG) materials, are artificial materials which consist of periodical scattering inclusions embedded in a homogeneous background. A great deal of attention has been paid to this new class of acoustic materials over the past two decades,[1–13] due to their ability to modify the propagation of elastic waves by the creation of PnBGs. Two classes of PnCs have been reported according to their material compositions, namely air inclusions in solid background[13,14] and solid inclusions in solid background.[5,8,15] According to the geometry of the structures, three-dimensional (3D) PnC substrate,[16] two-dimensional (2D) PnC slabs,[5,17,18] and one-dimensional (1D) PnC strips[19–21] have also been reported, of which the 2D PnC slab and 1D PnC strip have become popular research topics because of the better ability to confine elastic energy provided by the 2D and 1D nature of the PnC slabs and PnC strips, respectively. Researchers have also reported the PnC slabs which can be operated in GHz frequencies,[22,23] giving PnCs a big boost towards applications in RF communications. The PnC has also been demonstrated as liquid sensors recently,[24–28] showing the great potential of PnC structure in sensing applications.

When defects are created on an otherwise perfect PnC, devices of various functionalities, such as resonators and waveguides, can be realized.[29–42] For example, magnified directional acoustic source can also be created based on the resonant cavity of 2D PnCs[34]; a waveguide can be realized by adding a line defect (e.g., removing one row of holes) to PnC structure[35]; point defect modes are created to have high Q resonance on a 2D PnC slab[43]; cavity-mode resonators can be formed by introducing a line defect in the form of a Fabry–Perot resonant cavity structure.[44,45] However, there is one problem in this kind of cavity-mode resonators, which is known as the mode mismatch between the cavity mode (mode existed in the Fabry-Perot cavity) and the evanescent propagating mode (mode existed in the surrounding PnC). Analogically to the well-known photonic crystals (PhCs), such mode mismatch leads to significant scattering loss and reduction in the Q factor,[46] because abrupt terminations of the resonant cavity scatter the incident energy to other directions instead of reflecting the energy backward.[47] Recently, the design of introducing alternate defects to the resonant cavity was proposed to reduce the scattering loss and enhance the Q factor by making the transformation between the cavity mode (mode existed in the Fabry-Perot cavity) and the evanescent propagating mode (mode existed in the surrounding PnC) more gradual.[48]

In this paper, we extend the study on the design, fabrication, and characterization of micromechanical PnC resonators utilizing alternate defects. In the previous paper,[48] four rows of air holes are removed to form the resonant cavity, making the cavity length (L) equal to $4a$, whereby a is the lattice constant (pitch) which means the distance between the centres of two adjacent holes of the PnC. In this study, we further vary L to include $2a$ and $3a$ to investigate the effect of L on the performance of the resonators. Furthermore, for each case of L, we also introduce alternate defects with different central-hole radii (r') to study the effect of r' on the performance of the resonators. The PnC slab used for

[a)]Author to whom correspondence should be addressed. Electronic mail: elelc@nus.edu.sg.

this study was made by etching a square array of cylindrical air holes using a CMOS-compatible process in a free-standing silicon plate with thickness of 10 μm. Both the displacement profiles under their respective resonant frequencies and the band structures of all the designed resonators are calculated using finite-element-modelling (FEM) method. The "flatness" of the band structure is quantitatively analysed by the standard deviation (σ) of the band, and an inverse relationship was found between σ and the Q factors for the designed resonators with alternate defects, due to the slow sound effect brought by flat bands which reduces the energy loss along the lateral direction (Y direction) and enhances the Q factor.

II. MODELLING AND DESIGN

In the phononic structure, phononic band gap can be formed when scattering inclusions arranged periodically in a homogeneous host material which causes waves in certain frequencies to be completely reflected by the structure. When defects are introduced to the PnC structure by making the radii of the central rows of inclusions different from the inclusions of the surrounding PnC structure or replacing the central two rows of inclusions by only one row of inclusions, the periodicity of the defect region is different from the surrounding PnC structure, thus making the wavelength of the Bloch wave in the defect region different from the surrounding phononic structure. As such, a resonant peak can then appear within the stop band to form a phononic resonator.

A. PnC band gap optimization

The method we adopt to numerically analyse the band structure is FEM, using a commercial software called COMSOL. The main principle behind the FEM of the band structure follows closely from the Newton's Second Law of motion. The wave equation is shown as

$$\rho(r)\frac{\partial^2 u(r,t)}{\partial t^2} - \nabla[C(r)\nabla u(r,t)] = F = 0. \tag{1}$$

In Eq. (1), $\rho(r)$ is the mass density and $C(r)$ the elasticity matrix, which are both periodic functions. Therefore, they can be expanded to a two-dimensional Fourier series. u is the solution vector which consists of displacements u_x, u_y, and u_z. In our study, we set $F = 0$ because the solutions we are looking for are the eigenvalues. From the Bloch theorem, we can get

$$u(r,t) = e^{i(k\cdot r-\omega t)}\sum_G u_{k+G}e^{i(G\cdot r)}, \tag{2}$$

where $\mathbf{k}$ is a wave vector in the irreducible Brillouin zone and $\mathbf{G}$ is the two-dimensional reciprocal lattice vector. Substituting Eq. (2) into Eq. (1), we can get

$$\sum_{G'}\left[C_{G-G'}(k+G)\cdot(k+G') - \omega^2\rho_{G-G'}\right]u_{k+G'} = 0, \tag{3}$$

where $C_{\text{G-G}'}$ and $\rho_{\text{G-G}'}$ are the Fourier transforms of $C(\mathbf{r})$ and $\rho(\mathbf{r})$, respectively. Upon Fourier Transform of Eq. (3), the resulting harmonic time dependence term, $\exp(i\omega t)$, can be factored out. The time derivative can then be replaced by $-\omega^2$, as shown as

$$\frac{\nabla\cdot c\nabla}{\rho}u = \omega^2 u. \tag{4}$$

As shown in Eq. (4), the mode frequencies can be derived from the eigenvalues, ω^2, which could be solved by FEM. The isotropic silicon crystal[49] has the elasticity matrix (C matrix) in the form of

$$C_E = \begin{Bmatrix} c_{11} & c_{12} & c_{12} & 0 & 0 & 0 \\ c_{12} & c_{11} & c_{12} & 0 & 0 & 0 \\ c_{12} & c_{12} & c_{11} & 0 & 0 & 0 \\ 0 & 0 & 0 & c_{44} & 0 & 0 \\ 0 & 0 & 0 & 0 & c_{44} & 0 \\ 0 & 0 & 0 & 0 & 0 & c_{44} \end{Bmatrix}, \tag{5}$$

whereby

$$\begin{cases} c_{11} = 16.57\times 10^{10}\,\mathrm{Nm}^{-2} \\ c_{12} = 6.39\times 10^{10}\,\mathrm{Nm}^{-2} \\ c_{44} = 7.956\times 10^{10}\,\mathrm{Nm}^{-2} \end{cases}.$$

The detailed procedure of FEM and the band structure obtained for pure silicon PnC structure were described in Ref. 45 with a being the lattice constant (pitch) which means the distance between the centres of two adjacent holes, d being the thickness of the PnC slab, and r being the radius of the air holes. The value of d is fixed at 10 μm as it is the thickness of the device layer of the silicon-on-insulator (SOI) wafers used in the fabrication process. The values of a and r are chosen to be 18.18 μm and 8.18 μm after considering the theoretical optimization results reported in Ref. 50 and the limitation of our microfabrication capability. The optimized band structure has a stop band of 143.3 MHz $< f <$ 186.3 MHz, which renders the gap-to-midgap frequency ratio to be 26.1%.

B. PnC resonator structure design

The proposed PnC resonators are formed by alternately removing different number of rows of air holes ($L = \mathrm{n}a$, where n is the number of rows of air holes removed) at the centre of the otherwise perfect PnC structure. In addition to previously reported design of $L = 4a$, here we include another two types of resonators with three different L, i.e., $L = 2a$, $L = 3a$. For each type of L, we vary the radius of the central holes (r') from 2 μm to 8 μm, at a step of 2 μm. Therefore, for each type of L, there are four different cases of r', namely 2 μm, 4 μm, 6 μm, and 8 μm. The fabrication process which realized the designed resonators has already been reported in our previous work.[45] Fig. 1(a) shows the SEM image of the perfect PnC structure while the SEM images of the proposed alternately defected PnC resonators with different L are shown in Figs. 1(b)–1(d). Here, we only show the three cases of $r' = 4$ μm for the purpose of illustration. The insets of (b), (c), and (d) depict the close-up views of the resonant cavities of the three cases, respectively. Two sets of interdigital transducer electrodes are formed by Al on the

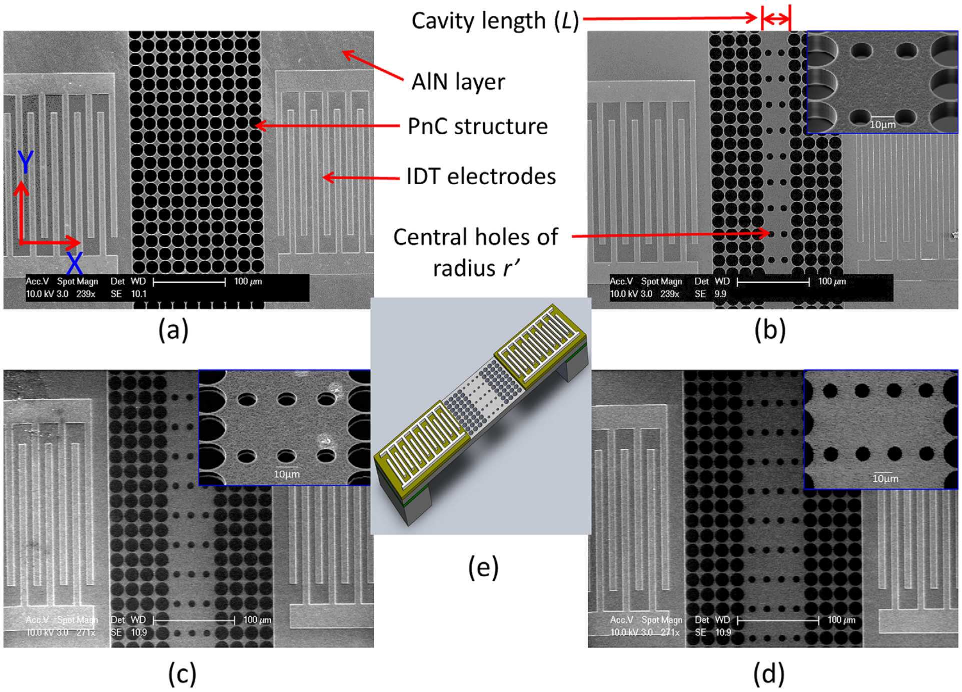

FIG. 1. SEM images of (a) the perfect PnC structure, (b) the alternately defected PnC resonator with $L = 2a$ and $r' = 4\,\mu$m, (c) the alternately defected PnC resonator with $L = 3a$ and $r' = 4\,\mu$m, (d) the alternately defected PnC resonator with $L = 4a$ and $r' = 4\,\mu$m. The insets of (b), (c), and (d) depict the close-up views of the resonant cavities of the three cases, respectively. (e) Schematic drawing of one of the designed devices.

two sides of the PnC structure. One set is used to launch waves along X direction while the other set is used to detect acoustic waves after their interaction with the phononic structure. The 3D schematic drawing which illustrates the design concept of the resonators is shown in Fig. 1(e).

III. DEVICE CHARACTERIZATION AND DISCUSSION

The experimental setup and the measurement procedure have also been reported previously.[45] The measured transmission spectra of some of the designed resonators, i.e., $L = 2a$ and $r' = 8\,\mu$m, $L = 3a$ and $r' = 8\,\mu$m, $L = 4a$ and $r' = 2\,\mu$m, are shown in Figs. 2(a)–2(c), respectively. From the measured transmission spectrum, the resonant frequency (f), the Q factor (Q), and the insertion loss (IL) for each designed resonator can be obtained. From the obtained f and Q, the $f.Q$ product is calculated by multiplying these two quantities with each other; From the obtained IL, the motional impedance (Z) is calculated according to the following equation when the resonator is directly connected to the 50-Ω terminations of the vector network analyser (VNA)[51]:

$$Z = 50 \times 10^{IL/20}. \tag{6}$$

The extracted parameters of all the designed resonators are summarized in Table I, where σ represents the standard deviation of the band of interest in the computed band structure of the designed resonator, which is a quantitative measurement of the "flatness" of the band and will be discussed in detail later in this section.

From Table I, we can see that for the case of $L = 2a$, both the resonant frequency and the Q factor increase with the increment in r', reaching 172.6 MHz and 1896, respectively. The IL reduces as r' increases, with the case of

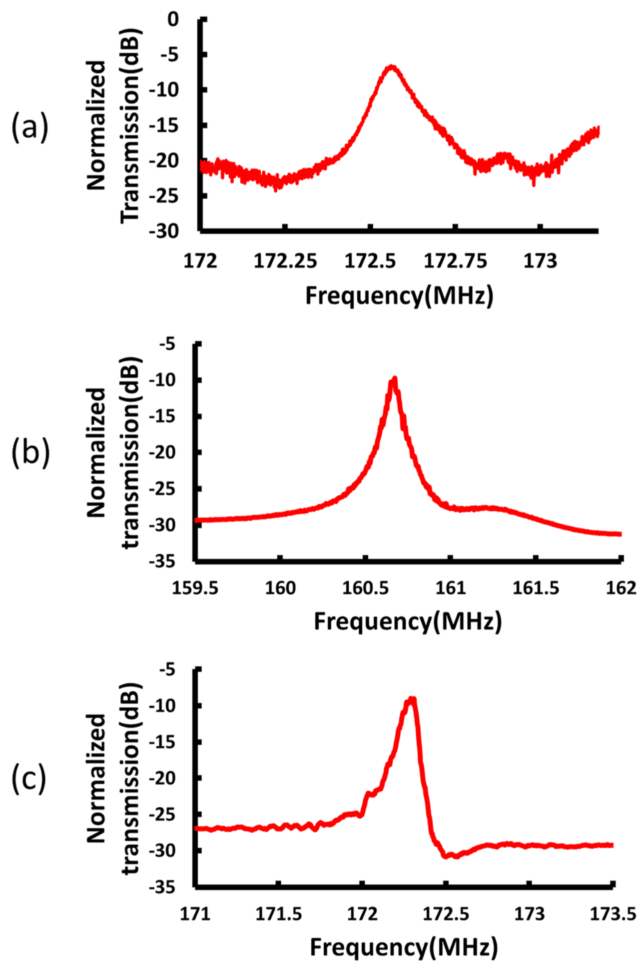

FIG. 2. Measured transmission spectrum of the alternately defected PnC resonator of (a) $L = 2a$ and $r' = 8\,\mu$m, (b) $L = 3a$ and $r' = 8\,\mu$m, (c) $L = 4a$ and $r' = 2\,\mu$m. The measured transmissions correspond to the cavity modes of $k_y = 0$.

TABLE I. Parameters of all twelve designs of resonators.

Cavity length (L)	r' (μm)	f (MHz)	Q	IL (dB)	f·Q (Hz)	Z (Ω)	σ (MHz)
2a	2	161.4	1242	14	2.00×10^{11}	251	3.43
	4	167.07	1392	10	2.33×10^{11}	158	3.19
	6	170.1	1780	8.6	3.03×10^{11}	135	1.18
	8	172.6	1896	6	3.27×10^{11}	100	1.09
3a	2	161.79	558	13.3	9.03×10^{10}	231	7.59
	4	162.19	2703	13.5	4.38×10^{11}	237	0.59
	6	158.1	289	18.3	4.57×10^{10}	411	5.97
	8	160.71	2009	10	3.23×10^{11}	158	0.64
4a	2	172.29	1914	8.96	3.30×10^{11}	140	1.05
	4	177.68	2221	8.33	3.95×10^{11}	130	0.92
	6	168.72	3039	3	5.13×10^{11}	71	0.38
	8	165.88	2074	7	3.44×10^{11}	112	0.96

$r' = 8\,\mu$m being the lowest, achieving 6 dB. For the case of $L = 3a$, the effects of r' on the resonant frequency, Q factor, and IL are different from the type of $L = 2a$. Both the resonant frequency and the Q factor fluctuate with the increment r': They increase when r' increases from 2 μm to 4 μm, and drop when r' further increases to 6 μm and bounce back to 160.71 MHz and 2009 when $r' = 8\,\mu$m. The IL has a slightly different trend: It increases until r' reaches 6 μm and reduces when r' further increases to 8 μm. As for the resonator with $L = 4a$, the resonant frequency increases as r' increases, reaching 177.68 MHz when $r' = 4\,\mu$m, which is the highest resonant frequency among all tested devices. The resonant frequency drops to 165.88 MHz when r' further increases to 8 μm; Q factor increases from 1914 to 3039, which is the highest among all the tested cases and it also yields a f·Q product of 5.13×10^{11}, when r' reaches 6 μm and it drops upon further increment of r'; IL has a similar trend as the Q factor: It reduces from 8.96 dB to 3 dB with the increment in r' until r' reaches 6 μm, and increases when r′ further increases to 8 μm. The trend of the resonant frequency with respect to r' is the same as the type of resonators with $L = 3a$ while the trend of the Q factor differs. It implies that the resonance condition of the PnC resonators with central-hole radius of 8 μm is slightly deviated from the optimized condition as achieved in the cases of r' of 6 μm.

To explain the effect of defect configuration on the Q factors, the band structures for all designed resonators are analysed using the aforementioned method. Fig. 3(a) is a reproduction of the band structure of the perfect PnC structure reported in our earlier work,[45] which shows a stop band of 143.3 MHz $< f <$ 186.3 MHz. This means no modes can exist within this frequency range and elastic waves whose frequency falls into the range of stop band cannot propagate through the PnC. Fig. 3(b) shows the band structure of the alternately defected PnC resonator with $L = 4a$ and with $r' = 8\,\mu$m. The band structures of all designed resonators are analysed but only the PnC resonator with $L = 4a$ and with $r' = 8\,\mu$m which typically represents the band structure of the alternately defected PnC resonator is shown here for the purpose of illustration. The calculated band structure shows the frequency against the reduced wave vector along the first irreducible Brillouin zone. By comparing Figs. 3(a) and 3(b), we observe that by having alternate defects on the otherwise perfect PnC structure, the band gap which exists in the perfect PnC structure disappears and there are some bands existed inside the original band gap. This means by having defects on the otherwise perfect PnC structure, modes can be supported in the frequency range of the original band gap as well.

In the band structure of the phononic structure, the first order derivative of frequency against wave vector represents the group velocity of guided mode of the elastic waves along the waveguide in the lateral direction. Therefore, modes associated with a flat band have a group velocity in Y direction equal or close to zero and exhibit strong spatial localization.[7] Elastic waves with small group velocity are called slow sound. Therefore, the phenomenon of the strong spatial localization of elastic waves due to small group velocity is also called the “slow sound effect.” On the other hand, a steep band means that the group velocity in Y direction is high. For the case of the cavity-mode resonator reported previously,[45] the two ends at the top and the bottom of the resonant cavity are open. In this case, when elastic waves enter the resonant cavity, its associated elastic energy can leak through the two open ends at the top and the bottom of the resonant cavity. Therefore, when the group velocity of guided mode along the waveguide in Y direction is high, the

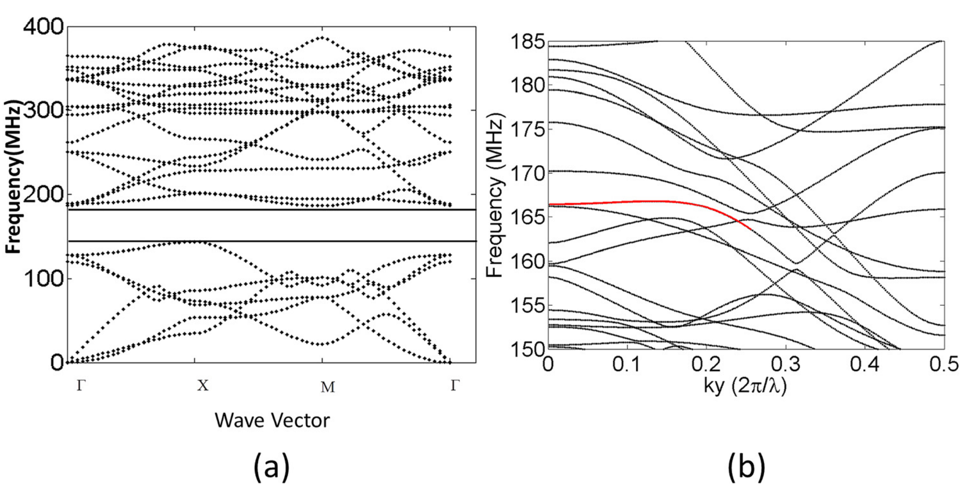

FIG. 3. Calculated band structure of (a) the perfect PnC structure, (b) the alternately defected PnC resonator with $L = 4a$ and with $r' = 8\,\mu$m.

rate of energy leakage and thus the energy loss is also high. On the other hand, when the group velocity of guided mode along the waveguide in Y direction is low or even zero, elastic waves hardly travel along Y direction and stay inside the resonant cavity to be reflected back and forth for a longer period of time, resulting in lower energy loss. Conceptually, the Q factor of a resonator is a direct indicator of the energy loss and is defined as

$$Q = \frac{2\pi \times EnergyStored}{EnergyDisipated}. \quad (7)$$

Therefore, the resonator with a flatter band (lower group velocity of guided mode along the waveguide in Y direction) should have a higher Q factor, due to lower energy loss. For the case of alternately defected PnC resonator with $L = 4a$ and with $r' = 8\,\mu$m, the band that corresponds to the resonant peak is the band which starts at 166.5 MHz when k = 0 [highlighted in red in Fig. 3(b)].

It has been reported that there are two types of slow modes existed in PhC waveguide.[52] The first slow mode exists near k = 0 and the second slow mode exists near k = 0.5. For the first slow mode (near k = 0), namely omni-directional reflection, the phase difference between the two surfaces of super cell under the periodic boundary conditions is 0° and light is reflected back and forth within the resonant cavity, forming a mode. It is obvious that such modes have very small forward component, i.e., they travel as slow modes along the waveguide direction, or for k = 0, form a standing wave. While for the second slow mode (near k = 0.5), namely coherent backscattering, the phase difference is 180° and the crystal acts as a one-dimensional grating. From our experimental results in Table I, the measured resonant frequencies of all the designed resonators are corresponding to the case of k = 0 as the eigenfrequency for k = 0 is very close to the measured resonant frequencies. Therefore, the slow sound modes for all the designed resonators correspond to the first slow mode, since PnCs are the acoustic wave analogy of the well-known PhCs.

Using the method mentioned in Sec. II A, we analysed the band structures of all twelve designed resonators and the bands of interest, which refer to the bands that correspond to the resonant peaks shown in Table I, are chosen and shown in the middle and the bottom figures of Figs. 4–6, respectively. All the top figures in Figs. 4–6 refer to the simulated static transmission field distributions of the displacement profile under the resonant frequency of the alternately defected PnC resonator, which will be discussed later in this section. We also show the first-order derivative of frequency against wave vector, which is essentially the group velocity of guided mode of the elastic waves along the waveguide in the lateral direction. Flatter bands lead to lower group velocity and steeper bands lead to higher group velocity. To analyse the "flatness" of the band quantitatively, we calculate

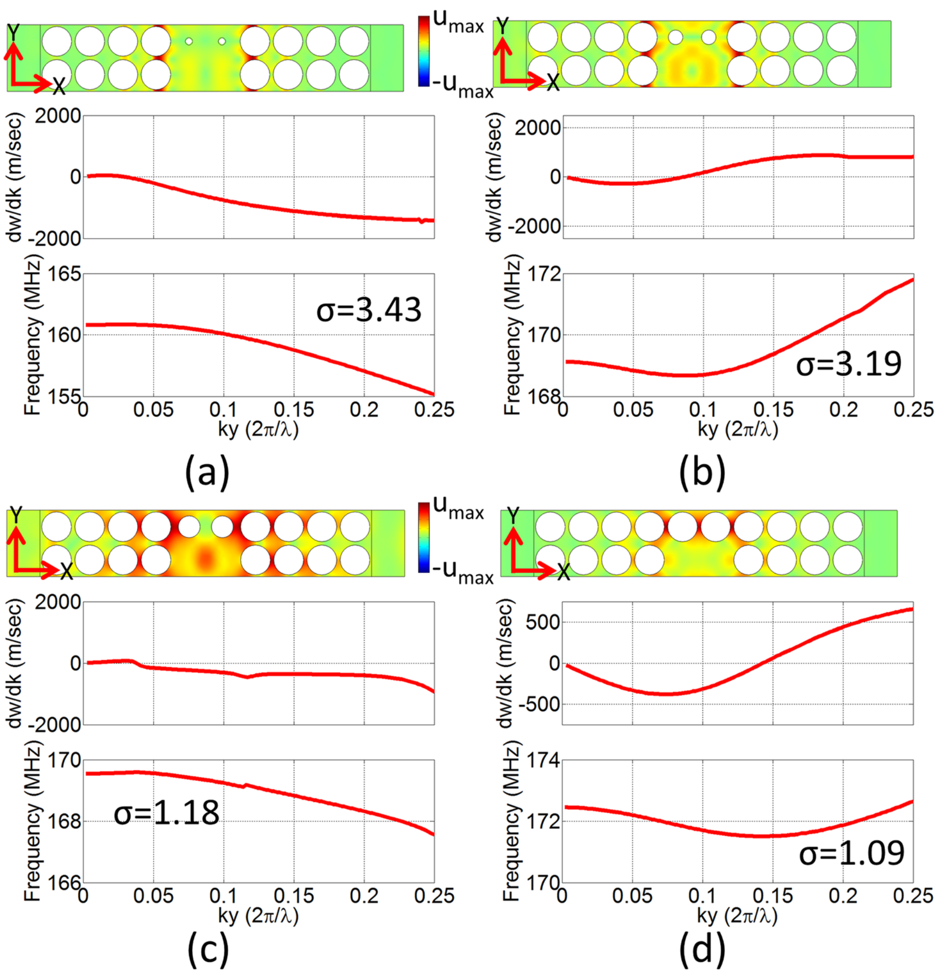

FIG. 4. The band structure which corresponds to the resonant peak (bottom figure), the first order derivative of frequency against wave vector (middle figure), and the simulated transmission field distributions of the displacement profile under the resonant frequency (top figure) of the alternately defected PnC resonator with $L = 2a$ and with (a) $r' = 2\,\mu$m, (b) $r' = 4\,\mu$m, (c) $r' = 6\,\mu$m, (d) $r' = 8\,\mu$m. The simulated field distributions correspond to the cavity modes of $k_y = 0$. The colour bar represents the amplitude and sign of the displacement.

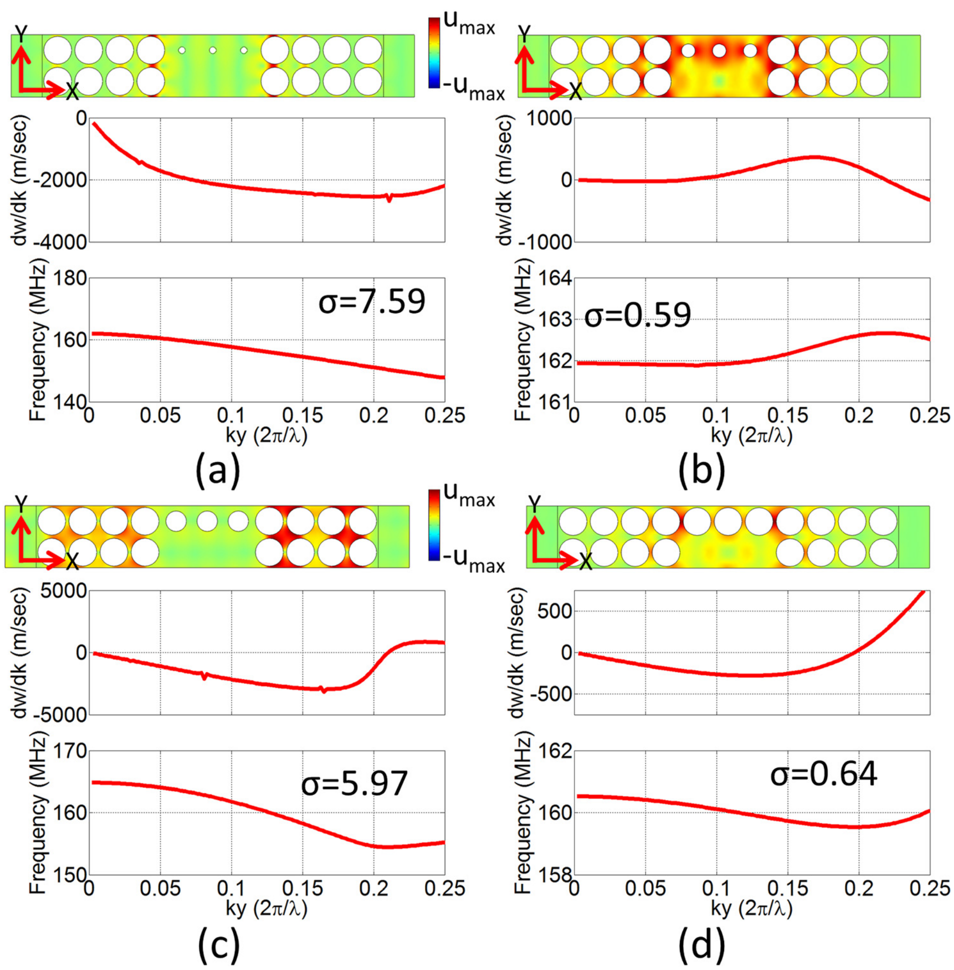

FIG. 5. The band structure which corresponds to the resonant peak (bottom figure), the first order derivative of frequency against wave vector (middle figure), and the simulated transmission field distributions of the displacement profile under the resonant frequency (top figure) of the alternately defected PnC resonator with $L = 3a$ and with (a) $r' = 2\,\mu$m, (b) $r' = 4\,\mu$m, (c) $r' = 6\,\mu$m, (d) $r' = 8\,\mu$m. The simulated field distributions correspond to the cavity modes of $k_y = 0$. The colour bar represents the amplitude and sign of the displacement.

the standard deviation (σ) of each band of interest and the values of σ are shown in Figs. 4–6 as well. As in our case, we sweep the value of k_y from 0 to 0.5 in steps of 0.002 and solve a series of eigenfrequencies for different values of k_y to get the band structure; therefore, for each of the band in the band structure, there are 250 data points representing the 250 different eigenfrequencies for these 250 values of k_y. As mentioned above, the slow modes in our experiment are near $k_y = 0$. Therefore, only the first 125 eigenfrequencies ($0 < k_y < 0.25$) are taken into the calculation of the standard deviation (σ), while the eigenfrequencies for the second slow sound mode ($0.25 < k_y < 0.5$) are not considered as they are not applicable in this study. As such, the standard deviation (σ) of a band can be obtained by calculating the standard deviation of the 125 eigenfrequencies for $0 < k_y < 0.25$. The smaller the σ, the flatter the band. The σ of all the designed devices is also summarized in the last column of Table I. Intuitively thinking, flatter bands should have smaller standard deviation. By calculating the standard deviation, we found that the simulation data explain the experimental results very well. For example, the alternately defected PnC resonator with $L = 4a$ and with $r' = 6\,\mu$m has the highest measured Q factor of 3039 among all the test devices, while it has the smallest calculated σ of 0.38, as shown in Fig. 6(c). We then plot the Q factors of all tested devices against their respective standard deviation of the band corresponding to the measured resonant peak (Fig. 7). We find that except two anomalous points, the measured Q factors are in an inverse relationship with the standard deviation of the corresponding band structure. The two anomalous points of exception could be due to variation of the hole size and lattice constant introduced in the microfabrication step.

In order to have a better visual understanding of the measured Q factors, the transmission field distributions of the displacement profiles of all designed PnC resonators under their respective resonant frequencies were analysed. Again, periodic boundary conditions are applied along Y direction. Elastic waves in silicon plate propagate by the interactions among the silicon atoms when they are displaced from their equilibrium positions. When atoms are displaced from the equilibrium positions, they can be modelled as spring systems and potential energy is then associated with the displacement. The potential energy stored is in a parabolic relationship with the displacement, according to the Hooke's law which describes the spring systems,

$$E_{potential} = \frac{1}{2}kx^2, \tag{8}$$

where $E_{potential}$ represents the potential energy stored in the structure, k is the spring constant, and x is the displacement from the equilibrium position. Therefore, the simulated displacement profiles actually represent the energy profiles distributed within the designed structure.

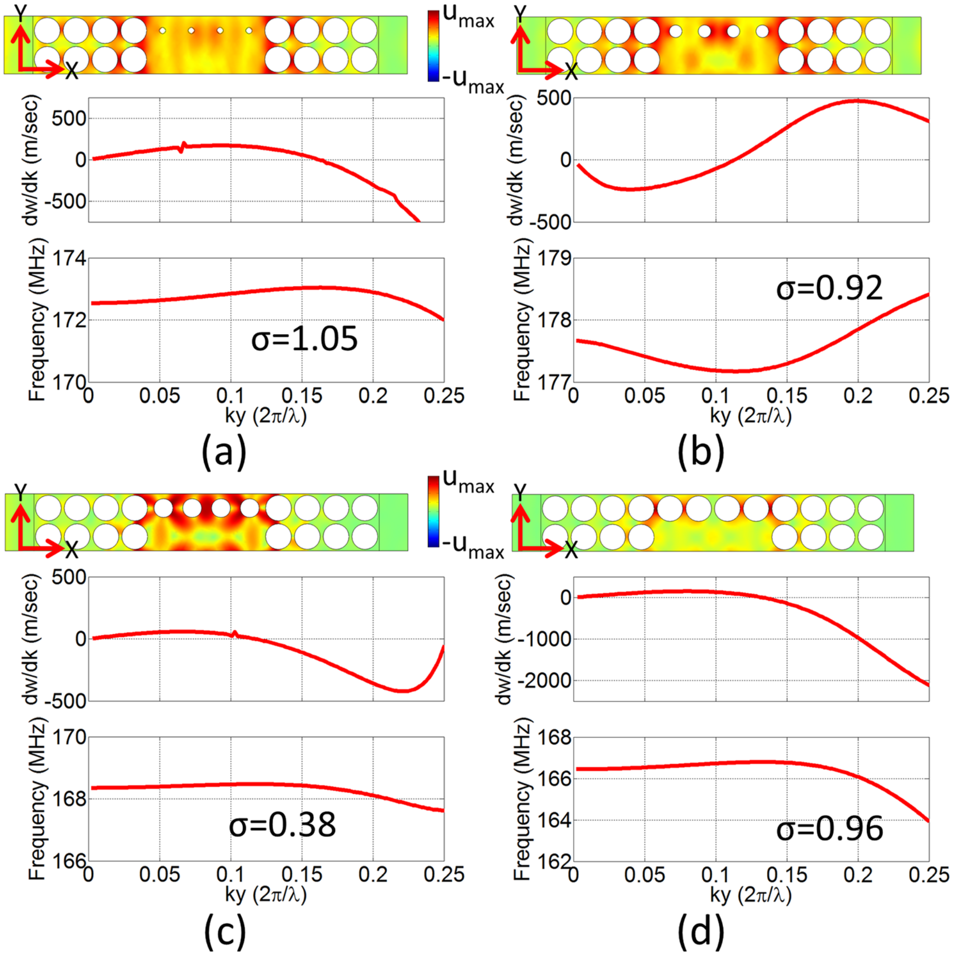

FIG. 6. The band structure which corresponds to the resonant peak (bottom figure), the first order derivative of frequency against wave vector (middle figure), and the simulated transmission field distributions of the displacement profile under the resonant frequency (top figure) of the alternately defected PnC resonator with $L=4a$ and with (a) $r'=2\,\mu$m, (b) $r'=4\,\mu$m, (c) $r'=6\,\mu$m, (d) $r'=8\,\mu$m. The simulated field distributions correspond to the cavity modes of $k_y=0$. The colour bar represents the amplitude and sign of the displacement.

All the top figures in Figs. 4–6 show the displacement profiles of the alternately defected PnC resonator with $L=2a$, $L=3a$, and $L=4a$, respectively. The colour bar in the middle of two displacement profiles indicates the amplitude and the sign of the displacements. If the amplitude of displacement, thus the elastic energy, is very large at the cavity region and very small at the surrounding PnC region, a higher Q factor can be expected as a result of the better confinement of the energy by the phononic structure surrounding the cavity. On the other hand, lower Q factor is expected for the cases whereby the displacement is very small at the central cavity region and very large at the surrounding PnC region, or evenly distributed along the structure. For these cases, the energy is confined poorly in the central cavity region, resulting in lower Q factor expected. The simulated displacement profiles are in good agreement with the measured data shown in Table I. For the four resonators with $L=4a$ (Fig. 4), the Q factor increases with the increment in r', as shown in Table I. The trend of Q factor as r' increases is very well reflected by the simulated displacement profiles. When $r'=2\,\mu$m, the displacement is large at the two edges of the resonant cavity while it is small inside the resonant cavity. When r' increases to $4\,\mu$m, although most of the displacements are still at the two edges of the cavity, the displacement inside the cavity also increases. This means that some of the energy is confined inside the cavity. Therefore, the Q factor increases from 1242 to 1392, as compared to the case of $r'=2\,\mu$m. When r' is further increased to $6\,\mu$m, more displacement, thus more energy, is concentrated inside the central cavity region. As a result, the Q factor is further increased to 1780. However, for this case ($r'=6\,\mu$m), the energy confinement in the cavity is not as good as the case of $r'=8\,\mu$m, as some of the energy leaks into the surrounding PnC region. The case of $r'=8\,\mu m$ has the highest Q factor among these four cases, as most energy is concentrated inside the cavity, especially around the edge of added central holes. At the same time, little energy leaks to the

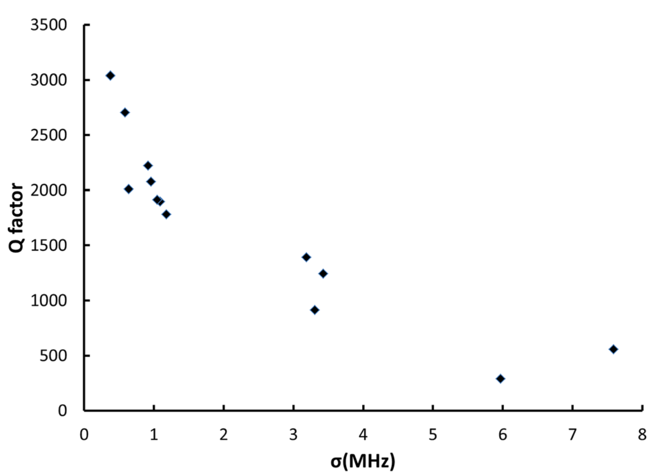

FIG. 7. Graph of Q factor against the standard deviation of the band that corresponds to the measured resonant peak for all designed alternately defected PnC resonators.

surrounding PnC region, making the energy confinement by the cavity very good. As a result, this case achieves the highest Q factor of 1896. Among all the twelve cases, the displacement vector components for the case of $L = 4a$ and $r' = 6\,\mu$m (Fig. 6(c)) are most concentrated at the central defect region, which means best confinement of energy by the surrounding PnC structure and thus the highest Q factor of 3039 was achieved by this design. On the other hand, in the case of $L = 3a$ and $r' = 6\,\mu$m (Fig. 5(c)), the displacement vector components and thus the energy are poorly confined within the central defect region, which leads to a lower measured Q factor of 289. Again, the confinement of energy which is represented by the simulated displacement profile is in very good agreement with the σ of the calculated band structure and confirms the inverse relationship between the σ of the calculated band structure and the measured Q factors.

IV. CONCLUSION

In this paper, development work of the alternately defected PnC resonators for 2D PnC structures was explored and characterized. Experimental data for twelve designs of PnC resonators with alternate defects based on square lattice PnC structure were reported. These designed PnC resonators of square lattice were fabricated from a free-standing silicon plate using a CMOS-compatible process. We have also characterized these resonators with different cavity length (L) and different central-hole radius (r') to explore the effect of L and r' on resonant frequency, Q factor, as well as IL. We quantitatively characterized the "flatness" of the band in terms of the band's standard deviation (σ) and found that the Q factors of the designed resonators are generally in an inverse relationship with σ. We also analysed the displacement profiles of all the resonators, which reflect the confinement of elastic energy within the resonant cavity and thus the expected Q factor. Agreement was also found between the calculated displacement profiles and the measured Q factors, which further confirms the inverse relationship between σ of the calculated band structure and the measured Q factors. Given the optimization results, the designed resonators are very promising to be further explored for various applications, such as microfluidics, biomedical devices, and RF communications.

ACKNOWLEDGMENTS

The authors would like to acknowledge the support by SERC Grant Nos. 1021010022 and 1021650084 from A*STAR, Singapore and National Science Council NSC100-2221-E-018-021, Taiwan.

[1] M. Sigalas, M. S. Kushwaha, E. N. Economou, M. Kafesaki, I. E. Psarobas, and W. Steurer, Z. Kristall **220**, 765 (2005).
[2] M. S. Kushwaha, P. Halevi, L. Dobrzynski, and B. Djafarirouhani, Phys. Rev. Lett. **71**, 2022 (1993).
[3] M. Sigalas and E. N. Economou, Solid State Commun. **86**, 141 (1993).
[4] R. Martinezsala, J. Sancho, J. V. Sanchez, V. Gomez, J. Llinares, and F. Meseguer, Nature (London) **378**, 241 (1995).
[5] I. El-Kady, R. H. Olsson, and J. G. Fleming, Appl. Phys. Lett. **92**, 233504 (2008).
[6] M. S. Kushwaha, P. Halevi, G. Martinez, L. Dobrzynski, and B. Djafarirouhani, Phys. Rev. B **49**, 2313 (1994).
[7] F. L. Hsiao, A. Khelif, H. Moubchir, A. Choujaa, C. C. Chen, and V. Laude, J. Appl. Phys. **101**, 044903 (2007).
[8] J. O. Vasseur, P. A. Deymier, B. Chenni, B. Djafari-Rouhani, L. Dobrzynski, and D. Prevost, Phys. Rev. Lett. **86**, 3012 (2001).
[9] H. Jia, M. Z. Ke, Z. J. He, S. S. Peng, G. Q. Liu, X. F. Mei, and Z. Y. Liu, J. Appl. Phys. **106**, 044512 (2009).
[10] X. F. Mei, G. Q. Liu, Z. J. He, L. B. Yu, Z. H. Yu, M. Z. Ke, and Z. Y. Liu, J. Appl. Phys. **107**, 064503 (2010).
[11] A. Khelif, F. L. Hsiao, S. Benchabane, A. Choujaa, B. Aoubiza, and V. Laude, in *Photonic Crystal Materials and Devices VII*, edited by A. Adibi, S. Y. Lin, and A. Scherer (SPIE-International Society for Optical Engineering, Bellingham, 2008), Vol. 6901, p. B9010.
[12] A. Khelif, F. L. Hsiao, A. Choujaa, S. Benchabane, and V. Laude, IEEE Trans. Ultrason. Ferroelectr. Freq. Control **57**, 1621 (2010).
[13] T. Gorishnyy, C. K. Ullal, M. Maldovan, G. Fytas, and E. L. Thomas, Phys. Rev. Lett. **94**, 115501 (2005).
[14] Y. Lai and Z. Q. Zhang, Appl. Phys. Lett. **83**, 3900 (2003).
[15] R. H. Olsson, I. F. El-Kady, M. F. Su, M. R. Tuck, and J. G. Fleming, Sens. Actuators, A **145**, 87 (2008).
[16] S. Benchabane, A. Khelif, J. Y. Rauch, L. Robert, and V. Laude, Phys. Rev. E **73**, 065601 (2006).
[17] S. Mohammadi, A. A. Eftekhar, A. Khelif, W. D. Hunt, and A. Adibi, Appl. Phys. Lett. **92**, 221905 (2008).
[18] S. Mohammadi, A. A. Eftekhar, W. D. Hunt, and A. Adibi, *Demonstration of Large Complete Phononic Band Gaps and Waveguiding in High-Frequency Silicon Phononic Crystal Slabs* (IEEE, New York, 2008).
[19] Z. L. Hou and B. M. Assouar, J. Phys. D: Appl. Phys. **42**, 085103 (2009).
[20] N. Gomopoulos, D. Maschke, C. Y. Koh, E. L. Thomas, W. Tremel, H. J. Butt, and G. Fytas, Nano Lett. **10**, 980 (2010).
[21] A.-C. Hladky-Hennion, C. Granger, J. Vasseur, and M. de Billy, Phys. Rev. B **82**, 104307 (2010).
[22] M. F. Su, R. H. Olsson, Z. C. Leseman, and I. El-Kady, Appl. Phys. Lett. **96**, 053111 (2010).
[23] Y. M. Soliman, M. F. Su, Z. C. Leseman, C. M. Reinke, I. El-Kady, and R. H. Olsson, Appl. Phys. Lett. **97**, 193502 (2010).
[24] M. Ke, M. Zubtsov, and R. Lucklum, J. Appl. Phys. **110**, 026101 (2011).
[25] R. Lucklum, J. Li, and M. Zubtsov, in *Eurosensor XXIV Conference*, edited by B. Jakoby and M. J. Vellekoop (Elsevier Science Bv, Amsterdam, 2010), Vol. 5, p. 436.
[26] R. Lucklum and L. Jing, in *IEEE International Ultrasonics Symposium (IUS)* (IEEE, 2009), p. 1154.
[27] R. Lucklum and J. Li, Meas. Sci. Technol. **20**, 124014 (2009).
[28] R. Lucklum, in *2008 IEEE International Frequency Control Symposium* (IEEE, 2008), p. 85.
[29] T. C. Wu, T. T. Wu, and J. C. Hsu, Phys. Rev. B **79**, 104306 (2009).
[30] S. Benchabane, A. Khelif, A. Choujaa, B. Djafari-Rouhani, and V. Laude, Europhys. Lett. **71**, 570 (2005).
[31] A. Khelif, P. A. Deymier, B. Djafari-Rouhani, J. O. Vasseur, and L. Dobrzynski, J. Appl. Phys. **94**, 1308 (2003).
[32] F.-L. Hsiao, A. Khelif, H. Moubchir, A. Choujaa, C.-C. Chen, and V. Laude, Phys. Rev. E **76**, 056601 (2007).
[33] A. Khelif, A. Choujaa, B. Djafari-Rouhani, M. Wilm, S. Ballandras, and V. Laude, Phys. Rev. B **68**, 214301 (2003).
[34] T. T. Wu, C. H. Hsu, and J. H. Sun, Appl. Phys. Lett. **89**, 171912 (2006).
[35] A. Khelif, S. Mohammadi, A. A. Eftekhar, A. Adibi, and B. Aoubiza, J. Appl. Phys. **108**, 084515 (2010).
[36] S. Mohammadi, A. A. Eftekhar, and A. Adibi, in *2010 IEEE International Frequency Control Symposium (FCS)* (IEEE, 2010), p. 521.
[37] M. Oudich, M. B. Assouar, and Z. Hou, Appl. Phys. Lett. **97**, 193503 (2010).
[38] Y. W. Gu, X. D. Luo, and H. R. Ma, J. Appl. Phys. **105**, 044903 (2009).
[39] M. B. Duhring, V. Laude, and A. Khelif, J. Appl. Phys. **105**, 093504 (2009).
[40] Z. Y. Liu, X. X. Zhang, Y. W. Mao, Y. Y. Zhu, Z. Y. Yang, C. T. Chan, and P. Sheng, Science **289**, 1734 (2000).
[41] J. O. Vasseur, A. C. Hladky-Hennion, B. Djafari-Rouhani, F. Duval, B. Dubus, Y. Pennec, and P. A. Deymier, J. Appl. Phys. **101**, 114904 (2007).
[42] Y. Pennec, B. Djafari Rouhani, H. Larabi, A. Akjouj, J. N. Gillet, J. O. Vasseur, and G. Thabet, Phys. Rev. B **80**, 144302 (2009).
[43] F. Li, J. Liu, and Y. H. Wu, J. Appl. Phys. **109**, 124907 (2011).
[44] S. Mohammadi, A. A. Eftekhar, W. D. Hunt, and A. Adibi, Appl. Phys. Lett. **94**, 051906 (2009).

[45]N. Wang, J. M. Tsai, F. L. Hsiao, B. W. Soon, D. L. Kwong, M. Palaniapan, and C. Lee, IEEE Electron Device Lett. **32**, 821 (2011).
[46]P. Lalanne and J. P. Hugonin, IEEE J. Quantum Electron. **39**, 1430 (2003).
[47]P. B. Deotare, M. W. McCutcheon, I. W. Frank, M. Khan, and M. Loncar, Appl. Phys. Lett. **94**, 121106 (2009).
[48]N. Wang, F.-L. Hsiao, M. Palaniapan, and C. Lee, Appl. Phys. Lett. **99**, 234102 (2011).
[49]B. A. Auld, *Acoustic Fields and Waves in Solids* (Wiley, New York, 1973).
[50]S. Mohammadi, A. A. Eftekhar, A. Khelif, H. Moubchir, R. Westafer, W. D. Hunt, and A. Adibi, Electron. Lett. **43**, 898 (2007).
[51]S. Pourkamali, G. K. Ho, and F. Ayazi, IEEE Trans. Electron Devices **54**, 2017 (2007).
[52]T. F. Krauss, J. Phys. D: Appl. Phys. **40**, 2666 (2007).